Dispersed Photovoltaic Generator with Flexible Interface

مولد فوتوفولطى منبث ذو وصلة قارنة مرنة

A. Elmitwally, member, IEEE and M. Rashed, member, IEE

Elect. Eng. Dept.,

Mansoura University,

Mansoura, 35516, Egypt

ملخص

تحظى نظم التوليد المنبث باهتمام متنامي فى الآونة الأخيرة لما لها من آثار جلية على تشغيل نظم القوى الكهربية وتعد مصفوفات الخلايا الشمسية الفوتوفولطية من أهم أنواعها ولذلك فإن هذا البحث يقترح وسيلة لتحسين اقتصاديات تلك النظم بتوسيع نطاق وظائف المغير الالكترونى الذى يربط مصفوفات الخلايا الشمسية الفوتوفولطية بالشبكة باستخدام أسلوب جديد للتحكم فيه يعتمد على مزيج من طريقتى المركبات الدوارة المتزامنة والمنطق المبهم تمكن المغير من استخلاص أقصى طاقة كهربية من الخلايا الشمسية و قمع التوافقيات وعدم الاتزان فى تيار الأوجه الثلاثة إضافة إلى إمداد الشبكة بالقدرة غير الفعالة وتنظيم جهد الربط العام، و قد تم التحقق من فعالية الطريقة المقترحة من دراسة أداء النظام عند ظروف تشغيل متنوعة عن طريق المحاكاة الديناميكية.

Abstract

The application of dispersed generation has a great attention nowadays due to its tangible impacts on the operation of distribution networks. Photovoltaic array is a significant type of embedded resources. This paper presents an approach to enhance the economics of dispersed photovoltaic generators. A control strategy is proposed to extend the functionality of its electronic converter interface to serve as a versatile power conditioner. Thereby, it can extract maximum power from the photovoltaic generator, eliminate harmonics, supply reactive power, suppress line current unbalance, and regulate the load voltage as ancillary tasks. The control algorithm is based on a hybrid synchronous reference frame-fuzzy logic scheme. The system performance is examined under a variety of operating situations and promising results are obtained.

Index Terms—Dispersed Generation, Photovoltaic Systems, Active Conditioners, Control, Fuzzy Logic.

I. INTRODUCTION

The need for more flexible electric systems with higher efficiency and quality, less environmental impact and with greater reliability motivates the development of dispersed generation (DG) and storage systems [1]-[10]. DG reduces the network losses, improve voltage profiles at consumer buses and defer T&D expansion investments. Meanwhile, it provides some operational challenges like protection devices mis-coordination, increased short circuit levels and degrading power quality [1].

The proliferation of nonlinear loads in distribution system causes increasing levels of harmonic distortion of current and voltage waveforms in the system. The introduction of DG makes the situation more serious. This results from the power electronic interface needed to integrate most of the DG types with the grid [11].

The power electronic interface may produce more harmonics and consume reactive power (e.g. SCR converters). So, an effective compensation system is required to maintain power quality [3].

Active power conditioners (APCs) are developed in the last two decades to improve power quality to permissible limits of the applied standards [12]. Recently, Distribution STATic COMpensator (DSTATCOM) has been applied to distribution networks to manage the system reactive power and to regulate the voltage [5].

For photovoltaic (PV) systems, the output power varies with the operating voltage even the insolation and temperature are constant. So, the output power of the PV array (PVA) may not be the maximum possible one for given insolation and temperature. This can worsen the economics of PV systems as the PVA with the highest component cost in the system is not fully utilised

in energy production. A maximum power point tracking (MPPT) scheme is always included to track the maximum output power operating point of the PVA [13].

In [11], the inverter interface of the DG integrated to the grid is concerned. A control method is presented that provides high quality of the DG current injected to the grid. A passive filter is designed and incorporated to attenuate the switching frequency components. A maximum power tracking system of PVA is described in [13]. It is based on boost dc chopper with feedforward control loop. In [14], the models of two DG sources, namely PVA and diesel-driven generation plant are formed. The co-ordinated management is introduced to fully exploit the PVA capacity. In [1] and [5], the concept of flexible distributed generation (FDG) is presented. A control strategy of the nonlinear link connecting DG to the distribution network using a current controlled voltage source inverter (VSI) is provided. FDG combines the functions of DSTATCOM and active power filter. It is able to compensate harmonics and reactive power in addition to active power conditioning and transfer to the grid. However, no specific DG source is studied. The dc bus output voltage of the arbitrary DG is considered as constant. This assumption is unrealistic for most of renewable DG resources, particularly PVA and wind turbines. Their output voltage and power fluctuate continuously as they depend on fairly random climatic factors.

This paper proposes a versatile nonlinear link to integrate the PV DG system to the grid. Its basic function is to regulate the active power flow from the PVA dispersed generator to the utility and to guarantee maximum output power extraction from the PVA at any climatic conditions. Besides, the link can supply reactive power to the utility to achieve any desired power factor operation or to stabilise the point of common coupling (PCC) voltage. Also, it can eliminate harmonics produced from nonlinear power, compensate three phase currents unbalance, and regulate the point of common coupling (PCC) voltage. Thus, the controlled converter interface replaces the PVA maximum power point tracker (MPPT), DSTATCOM, filters and on-load tap changing mechanism (OLTC) of the substation transformer. Accordingly, a great reduction in the system cost is attained. Hence, the proposed DG-supported APC, will be referred to as DGAPC, fits the operational needs of distribution networks.

II. SYSTEM CONFIGURATION

The general topology of the studied system is shown in Fig.1. A three-phase rectifier load is connected to a four wire 11 kV distribution grid through a matching transformer. The transformer is 11kV/380V (line voltage) with Wye-connected windings in both primary and secondary sides. The solar PVA dispersed source is coupled directly to the DC bus of its interfacing PWM converter via a small reactor. The later helps to stabilise the DC bus voltage. The converter is a three-phase three-leg half bridge PWM voltage-source current controlled IGBT converter. When a proper control strategy is adopted for this interface converter, it will undertake the dedicated compensation tasks discussed in the former section. Hence, it forms the core of the DGAPC presented in this paper. The dc bus uses a common split capacitor with a centre tap connected to the neutral line. The ac side of the DGAPC is shunt connected to the PCC through a synchronous link reactor, L, which contributes also as a first order filter. Owing to this topology, the three phases can be regarded as three decoupled single phases permitting the implementation of per-phase current controllers. The converter model is provided in [12]-[14].
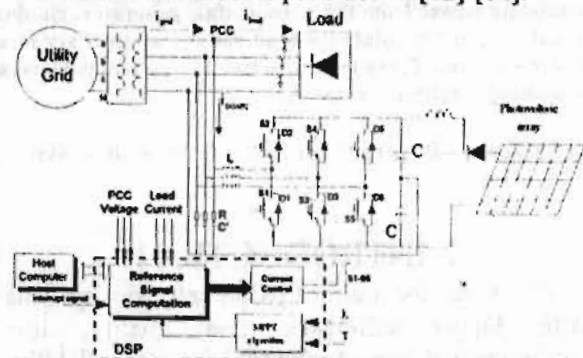

Fig.1. The System configuration.

III. THE PHOTOVOLTAIC ARRAY

The PV technology for the utilisation of solar energy is one of the most attractive renewable resources. It is featured by a high investment cost for its application. The typical structure of a PVA is constituted by a high number of modules arranged in a parallel and series connections to give the desired voltage and current outputs. The PVA studied herein consists of 150 series-connected and 10 parallel-connected modules that produces about 70 kW at 1750 V for a solar insolation of 1000 W/m^2 and a temperature of 25

C^o. The nonlinear voltage-current characteristics of the PVA and the output power for insolation levels of 100 to 1000 W/m^2 and at a step of 100 W/m^2 T=25 C^o is depicted in Fig.2.

It is economically inevitable to extract the maximum available power of the PVA. The output power of the PVA varies with its operating DC voltage at certain insolation and temperature. The maximum output power occurs at 60-70% of the open circuit voltage of the PVA. The output power surely changes with the climatic conditions of solar insolation level (λ) and the ambient temperature (T). The model and the data used for the PVA modules are taken from recent papers [13]- [15].

For the purpose of the proposed DGAPC, it is targeted to be capable of tracking the maximum output power from the PVA. Therefore, the operating DC voltage of the PVA that will provide maximum output power has to be determined for given values of λ and T. This voltage value will be considered as the setting value of the PWM converter DC bus voltage that is taken as an input to DGAPC control scheme. There are several means to specify the operating DC voltage that ensures maximum output power production from the PVA [14]. Multivariable linear regression technique and feedforward neural networks are used alternately in this study. For many different possible combinations of λ and T, the corresponding maximum output power operating DC voltage values are computed via the mathematical model of the PVA. This obtained data is used to estimate the coefficients of the regression model which correlates the maximum output power operating DC voltage $V_{max\,p}$ to λ in W/m^2 and T in C^o as inputs. The model is described in (1).

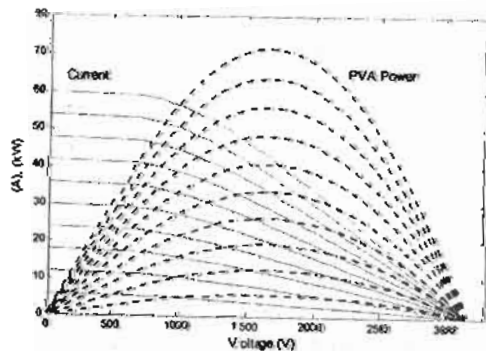$$V_{max\,p} = a_1 \sqrt{\lambda} + a_2 T + a_3 \qquad (1)$$

Fig. 2. The PVA characteristics.

The same data is used to design and train the feedforward neural network (FFNN) that has two input neurons (for λ and T), and one output neuron (for $V_{max\,p}$). The FFNN has 12 neurons in the hidden layer with segmoid transfer function [16]. After training, the FFNN fits indirectly the relation between the input variables and the output variable. The estimation error for the regression model is below 5% and it is less than 3% for the FFNN.

IV. THE PROPOSED SCHEME

The proposed control strategy of the DGAPC is based on a hybrid synchronous reference frame (SRF)- fuzzy logic system. It is composed of three loops as shown in Fig.3. They are described in the following subsections.
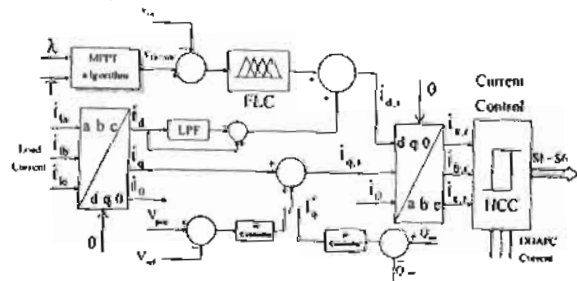

Fig.3. Schematic diagram of the DGAPC control system

A.. The Main Loop

The sensed three-phase load currents are converted into three components (i_d, i_q and i_0) in the rotating d-q-0 reference frame at a transformation angle θ via (2).

$$\begin{bmatrix} i_d \\ i_q \\ i_0 \end{bmatrix} = \sqrt{\frac{2}{3}} \begin{bmatrix} \cos\theta & \cos\left(\theta - \frac{2\pi}{3}\right) & \cos\left(\theta - \frac{4\pi}{3}\right) \\ -\sin\theta & -\sin\left(\theta - \frac{2\pi}{3}\right) & -\sin\left(\theta - \frac{4\pi}{3}\right) \\ \frac{1}{\sqrt{2}} & \frac{1}{\sqrt{2}} & \frac{1}{\sqrt{2}} \end{bmatrix} \begin{bmatrix} i_a \\ i_b \\ i_c \end{bmatrix} \qquad (2)$$

θ is the angular position of the rotating reference frame. θ is produced from the sensed three-phase grid voltages using a phase locked loop PLL [11]. The fundamental frequency component is converted by this transformation into a dc quantity and the non-fundamental ones are involved as ripples. The d and q axis currents are composed of a dc component and ripples expressed as

$$i_x = \bar{i}_x + \tilde{i}_x \qquad (3)$$

where x denotes to d or q axis, $\bar{i}_x$ is the dc current component and $\tilde{i}_x$ is the ripple.

Extraction of the dc component, as a crucial step, is effectively accomplished by a low-pass filter

(LPF). A third order Butterworth LPF with a cut-off frequency of 20 Hz is adequate. LPF provides no phase errors for dc signals.

B. The Maximum Power Tracking Loop

Flexibility, robustness, insensitivity to parameter variation and nonlinearity handling capability are powerful advantages in fuzzy logic controller (FLC). Therefore, FLC is selected instead of the conventional PI controller in this maximum power tracking loop [12]. The actual DC bus voltage is sensed and compared to a dynamic setting point computed from either from (1) or FFNN discussed in the previous section. The difference ΔV_{DC} is processed in a well-designed FLC to yield the correction component ($i_{d,max\,p}$) that is added to the load d-axis current i_d to produce the d-axis reference current of the DGAPC ($i_{d,r}$). The construction of the FLC block of Fig.3 is shown diagrammatically in Fig.4.
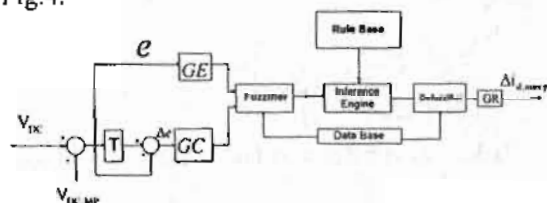

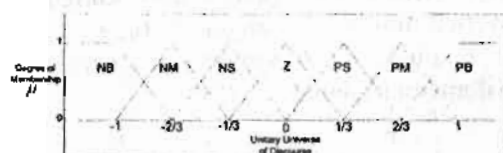Fig.4. Structure of Fuzzy Logic DC Voltage Controller.

Fig.5. Shape of membership functions.

The fuzzy control algorithm consists of a set of fuzzy control rules which reflects the experience gained from the plant operation. The rules are combined by using the implication and the compositional inference [12]. The presented fuzzy controller has two inputs and one output. The first input is the DC bus voltage error (e) and the second is the change in the DC bus voltage error (Δe). The output is the change in the d-axis reference current component of the DGAPC that will verify maximum power extraction of the PVA, $\Delta i_{d,max\,p}$. The membership functions are triangular shaped with 50% overlap for a soft and progressive control adjustment (see Fig.5). Each variable has 7 membership functions labelled from negative big (NB) to positive big (PB). Fig.5 depicts the unitary universe of discourse adopted

for the all three control variables. It can be modified by a simple gain for each variable, GE for e, GC for Δe and GR for $\Delta i_{d,max\,p}$ (see Fig.4). A rule base of 49 rules is selected to establish the fuzzy controller [5], [12]. With the use of Mamdani's implication and with defuzzification by a centroid method [12], the fuzzy controller provides the value of $\Delta i_{d,max\,p}$. For the time sample number k, the value of $i_{d,max\,p}$ is given in (4) as:

$$i_{d,max\,p} = i_{d,max\,p}(k-1) + GR\,\Delta i_{d,max\,p} \qquad (4)$$

C. Reactive Current Adjustment Loop

The DGAPC controller is supplemented by a third loop dedicated to regulate alternately either the PCC voltage or the reactive power flow to the grid. It is composed of two branches. The first forces the DGAPC to inject adequate amount of fundamental reactive current with relevant sign into the power line. This current builds correcting voltage drop across the utility grid system impedance to regulate the PCC voltage. The peak PCC voltage (V_{PCC}) is compared to its reference value (V_{ref}). The error is processed in a PI controller to give a corrective fundamental reactive current $i_{q,VR}$ that is summed up with the q-axis component of the load current. The second branch caters for regulating the reactive power flowing into the grid. An amount of current which represents a desired setting for supplying reactive power to the grid (i_q^*) is added as shown in Fig.3. The reactive power flow to the grid is compared to its setting value. The error is processed in a PI controller to give the corrective fundamental reactive current i_q^* that is summed up with the q-axis component of the load current.

D. PWM and Current Control

The three loops described above are integrated as revealed in Fig.3. The net d, q and 0 components of the DGAPC reference currents, $i_{d,r}$, $i_{q,r}$ and i_0, are used to obtain the phases a, b and c reference currents of the DGAPC, $i_{a,r}$, $i_{b,r}$ and $i_{c,r}$, through the inverse transformation [1], [11]. The sampled three error signals initiated by comparing the three-phase reference currents to actual DGAPC three-phase output currents are used to generate the switching

patterns of the six IGBT switches of the converter via a hysteresis current controller (HCC) as depicted in Fig.3. When the error exceeds the limits specified by the hysteresis comparator, the switching state of the IGBTs in the corresponding phase leg of the converter is reversed to minimise the error tracking the reference template. The main shortcoming of the classic HCC is that the switching frequency, beside its dependency on the band limits, is usually prohibitively very high and varying. To alleviate this aspect, the errors in DGAPC currents are sampled at constant rate of 20 kHz before entering the HCC. This assures that the maximum switching frequency is less than 20 kHz which is suitable for high power IGBT switches.

TABLE I
SYSTEM PARAMETERS USED IN SIMULATION

Utility	Voltage:11 kV (line), Frequency: 50 Hz
PVA	Terminal smoothing reactor= 20 mH $a_1 = -15.92$, $a_2 = 6.86$ and $a_3 = 1858.54$
DGAPC	C = 10000 µF, L = 2 mH, maximum switching frequency $\cong$ 20 kHz,
Rectifier load	L=20 mH, R= 2Ω Unbalance load: 4 Ω, 8 mH
RC Branch	R = 2Ω, C'= 50 µF

V. PERFORMANCE OF THE DGAPC

The proposed DGAPC is examined for achieving maximum power extraction of the PVA, harmonics elimination, power factor correction, line currents unbalance removal and voltage regulation under three different operating conditions. They are described in the following three subsections. The attained amendment in the waveforms is evaluated in terms of total harmonic distortion (THD) of line current and PCC voltage. The load is composed of three phase diode bridge rectifier with R-L load. The proposed DGAPC is simulated in MATLAB environment. A list of the system parameters considered in simulation is listed in Table I. The ambient temperature is assumed as 25 C°.

The investigation results are indicated in Table II. The case index in this table refers to the

operating condition set as pointed out in the following subsections A-C sequentially. For the first two cases the voltage regulation control branch is put out of action to enable unity power factor operation of the grid source.

A. Balanced Load Conditions
Figs.6 and 7 show the performance of the DGAPC under these conditions. The insolation is assumed to be constant at 1000 W/m². Fig. 6 depicts the following from top to bottom: (a)the three-phase load currents, (b) the three phase grid currents, (c) the three phase DGAPC currents, and (d)the load and the grid current spectra of phase a, where load current spectrum is in the dotted line, and the grid current spectrum is the solid line.
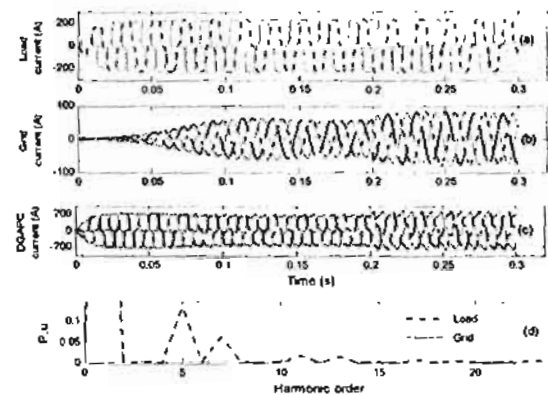

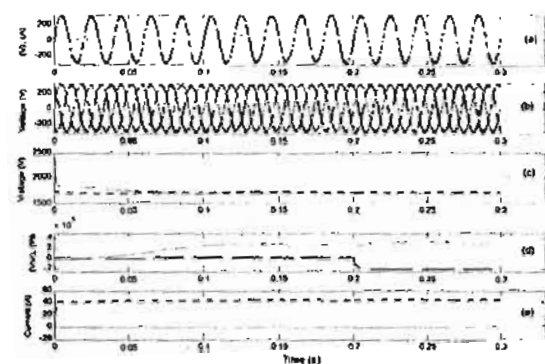Fig.6. Current waveforms at balanced condition.

Fig.7. DGAPC performance at balanced condition.

Whereas Fig. 7 reveals the following:
(a) the phase a line to neutral voltage at PCC and grid current versus time, (b) the three-phase PCC voltages, (c) the reference DC bus voltage decided by the MPPT FFNN and the actual DC bus voltage., (d) the three-phase grid-supplied active and reactive power where the reactive one is the

dotted line., and (c) the PVA output current (the dotted line) and the neutral line current.

From these figures, it is noticed that the grid current is nearly sinusoidal and in phase with the phase voltage resulting in near-unity power factor operation. The DGAPC has been able to suppress all the individual load current harmonics. The unity power factor is manifested only for the time before 0.2 s where a step change in the grid reactive power setting from 0 to 20 kVars occurs (Fig.7 d). The DGAPC exhibits good dynamic response within a less than half period of the fundamental frequency (10 ms). The DC bus voltage is approximately maintained constant at the value decided by the FFNN MPPT algorithm. The three-phase line currents are almost sinusoidal and balanced with the proposed DGAPC. The neutral line current is nearly zero. The PVA supplies about 70 kW which is its maximum output as dictated by the MPPT algorithm. On the other hand, the grid delivers additional 40 kW (Fig.7 d) to meet the load power requirements.

B. Unbalanced Conditions

An extra R-L load is connected between phase a and the neutral at PCC. The system performance for that case is demonstrated in Figs. 8 and 9which are analogical to Figs.6 and 7 described in the above subsection. The total load currents are unbalanced as shown in Fig.8a with unbalance ratio of 10.2%. The rms value of the phase voltage is 220 V. The three-phase grid currents are shown in Fig. 8b. The grid currents are forced to be approximately balanced. Their unbalance ratio has been suppressed to less than 0.5%. The neutral line current as shown in Fig.9e tends to zero.The grid currents are almost sinusoidal with unity power factor relative to the respective phase voltage. When a step change from 1000 W/m^2 to 500 W/m^2 occurs to the insolation at 0.2 s, a momentarily short circuit happens to the PVA (Fig.9d). Its output power comes down to about 35 kW. The grid active power is increased through a transient period of 6 cycles to 65 kW to support the load compensating the deficiency in the PVA output power. This is also reflected in the grid currents where they are nearly doubled. The DC bus voltage comes back to its reference value in about 5 cycles.
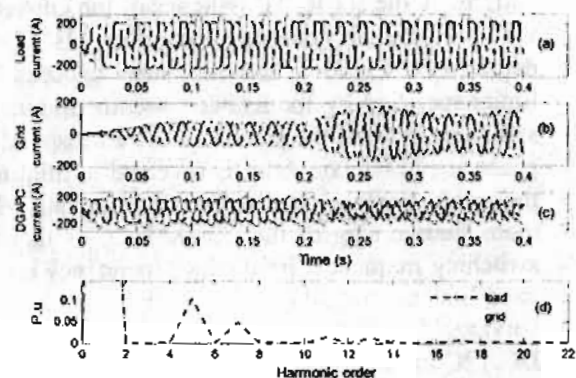

Fig.8. Current waveforms at unbalanced condition.

c. Voltage Regulation

The DGAPC is capable of accomplishing voltage regulation at PCC by managing the requested voltage drop across the utility power system impedance. This is revealed in Figs.10 and 11, where the voltage regulation control branch as discussed in section 4 is enabled while the reactive power control branch is suspended.

Fig.10 is equivalent to Fig.6 but an insolation level of 700 W/m^2 is considered in this case. A step change in the phase a load occurs at 0.15 s to bring unbalance in the three phase load currents.

Fig.11 is similar to Fig.7 except that the peak (dotted line) and rms values of the three phase voltages at PCC are depicted in Fig.11c. The DGAPC maintained the PCC rms voltage (its output voltage) at 220V for all time even after the load is increased and becomes unbalanced at 0.15 s (Fig.11c). Before the time0.15 s, the reactive power flow to the grid is negligible (unity power factor operation). After that time, considerable amount of reactive power (about 20 kVars) flows to the grid from the DGAPC as a side product of the PCC voltage regulation process (Fig.11d) .
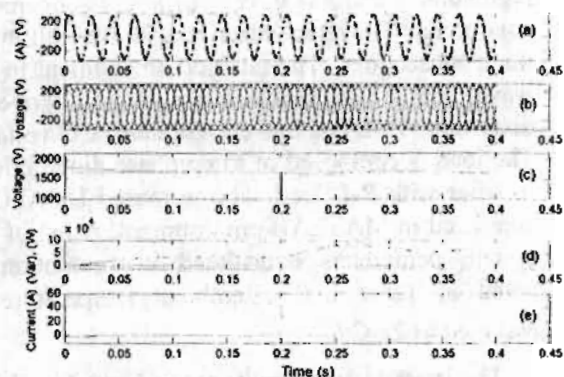

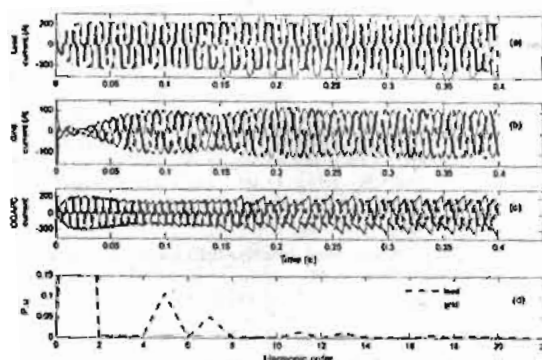Fig.9. DGAPC performance at unbalanced condition.

Fig.10. Current waveforms for voltage regulation case.

The voltage control loop responds in about 2 ms from starting to stabilise the PCC voltage (Fig.11b and Fig.11c). It is immune to sudden variations in load keeping constant PCC voltage. This illustrates that the proposed DGAPC does a good job in stabilising the PCC voltage. It can be remarked from Fig.10b that the three phase grid currents are harmonic free and balanced for all time.

TABLE II
PERFORMANCE OF THE DGAPC EXPRESSED IN THD%

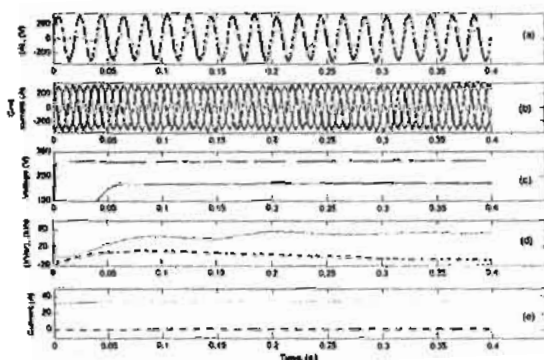| Case	Load current	Grid current	PCC voltage
A	15.32	1.68	3. 55
B	12.01	0.96	3.13
C	12.07	1.67	3.09

Fig.11. DGAPC performance for voltage regulation mode.

VI. CONCLUSION

A flexible PV DG supported active power conditioner (DGAPC) is presented in the paper. Its target functions are to regulate the active power flow supplied from the PVA dispersed generator to the utility and to extract maximum output power from the PVA at any climatic conditions. Furthermore, the link can supply reactive power to the utility to achieve any required power factor operation or to sustain point of common coupling (PCC) voltage. Also, it can eliminate harmonics, and compensate three phase currents unbalance. This package of functions is accomplished through the proper control scheme of the PWM converter interfacing the PVA to the utility. A hybrid SRF-FLC scheme is adopted to determine the reference signals of the DGAPC and hysteresis current control is used to produce the switching patterns of its IGBT switches. The system is investigated under different operating conditions and simulation results are discussed. The efficacy of the studied approach has been verified. The DGAPC is found to be competent in accomplishing its compensation tasks. It also has a high dynamic response within half a cycle.

VII. REFERENCES

[1] Mostafa I. Marei, Ehab EL-Saadany and Magdy M. A. Salama, "Flexible Distributed Generation: (FDG)," IEEE PES Summer Meeting, 2002, pp.49-54.

[2] G. Celli, F. Pilo, "Optimal Distriuted Generation Allocation in MV Distribution Networks," IEEE PES Summer Meeting, 2001, pp.81-86.

[3] Z. Chen, F. Blaabjerg and J. K. Pedersen, "A Hybrid Compensation System with an Active Filter and Distributed Passive Filters in Power Systems with Dispersed Generation," IEEE PESC'003, 2003, pp. 767-772.

[4] Ding Xu and Adly Girgis, "Optimal Load Shedding Strategy in Power Systems with Distributed Generation," IEEE PES Summer Meeting, 2001, pp.788-793.

[5] Mostafa I. Marei, Ehab EL-Saadany and Magdy M. A. Salama, "A Novel Control Algorithm for the DG Interface to Mitigate Power Quality Problems," IEEE Transactions on Power Delivery, Vol. 19, No. 3, pp. 1384-1392, July 2004.

[6] S. Matsushita, K. Yukita, Y. Goto, K. Ichiyanagi, H. Aoki and Y. Mizutani, "Automatic (d) ation Control using GA Considering Distributed Generation," IEEE PES Summer Meeting, 2002, pp. 1579-1583.

[7] Tac-Eung Kim and Jae-Eon Kim,"Considerations for the Feasible operatin range of Distributed Generation Interconnected to Power Distribution Systems," IEEE PES Winter Meeting, 2002, pp. 42-48.

[8] Thomas Ackermann and Valery Kanyazkin, "Interaction between Distributed generation and the Distribution Network: Operation Aspects," IEEE PES Summer Meetin, 2002, pp.137-1362.

[9] Pathmothat Chiradeja and R. Ramakumar, "An Approach to Quantify the Technical Benefits of Distributed Generation," IEEE Trans. On Enery Conversion, Vol. 19, No.4, pp. 764-773, Dec. 2004.

[10] Il-Yop Chung, Sung-Woo Park, Hee-Jung Kim, Seung-Il Moon, Byung-Moon Han, Jae-Eon Kim and Joon-Ho Choi, "Operating Strategy and Control Scheme of Premium Power Supply Interconnected with Electric Power Systems," IEEE Trans. On Power Delivery, Vol.20, No.3, PP. 2281-2288, July 2005.

[11] Milan Prodanovic and Timothy Green, "Control and Filter Design of Three-Phase Inverters for High Power Quality Grid Connection," IEEE Transactions on Power Electronics, Vol. 18, No. 1, pp.373-380, Jan. 2003.

[12] Juan Dixon, Jose Contrado and Luis Moran, "DC Link Fuzzy Control of an Active Power Filter, Sensing the Line Current Only" Conference Record of IEEE PESC, 1997, pp.1109-1114.

[13] Mikihiko Matsui, Tatsuya Kitano, De-hong Xu and Zhong-qing Yang, "New Maximum Photovoltaic Power Tracking Control Scheme Based on Power Equlibrium at DC Link," Conference Record of 34th IEEE IAS Annual Meeting, Oct. 1999, pp. 804-809.

[14] D. Canever, G. Dudgeon, S. Massucco, J. Mc Donald and F. Silvestro, " Model Validation and Coordinated Operation of a Photovoltaic Array and a Disel Powe Plant For Distributed Generation," IEEE PES Winter Meeting, 2001, pp. 626-631.

[15] A. Oliva, J. Balda, D. McNabb and R. Richardson, "Power-Quality Monitoring of a PV Generator," IEEE Transactions on Energy Conversion, Vol. 13, No. 2, pp. 188-193, June 1998.

[16] Yaow-Ming Chen, Robert M. O'Connell: "Active Power Line Conditioner with a Neural Network Control," IEEE Transactions on Industry Applications, Vol.33, No.4, pp.1131-1136, 1997.

VIII.BIOGRAPHIES

Akram Elmitwally (member IEEE) was born in Dakahlya, Egypt in 1967. He obtained B.Sc, M.Sc and Ph.D in 1989, 1995 and 2002, respectively. All are in electrical power engineering from Mansoura university, Egypt. He has been a visiting researcher at the electronic and electrical engineering department, university of Bath, UK between 1998 and 2000. Currently, he is a lecturer at the electrical engineering department, Mansoura university, Egypt. His fields of interest include power quality, power system transients, dispersed generation and AI applications in energy systems.

Mohamed Rashed (member IEE) was born in Dakahlya, Egypt in 1965. He obtained B.Sc, M.Sc in electrical engineering from Mansoura university in 1987 and 1993. He obtained Ph.D in electrical drives from Abrdeen university, UK, in 2002. He has been a post doctoral fellow at the department of engineering, university of Abrdeen, UK between 2002 and 2005. Currently, he is a lecturer at the electrical engineering department, Mansoura university, Egypt. His fields of interest include the development of novel algorithms to AI-based self tuning, sliding mode, adaptive inverse and sensorless control of electrical drives and grid-connected renewable energy resources.

An Efficient Contour based Shape Descriptor
For Representation and Classification of Medical Images

واصف كفؤ للشكل مبنى على المخطط الخارجى لتمثيل وتصنيف الصور الطبية

Saad M. Saad	Shawkat K. Guirguis	Ashraf M. Emam
Assistant Lecturer	Assoc. Professor	Assistant Professor

Department of Information Technology, Institute of Graduate Studies and Research
University of Alexandria
P.O. Box 832, El Shatby 21526, Alexandria, Egypt.

الملخص العربي

ابتكار مصنف قوى للصور الرقمية يعتمد على أستحداث واصفات دقيقه مستقاة من المحتوى المرئــى للصورة . و واصفات الشكل القائمة على المخطط الخارجى توظف فى التمثيل المبنى على الأشياء و ذلك يرجع إلى إمكانيه تطبيقها على الأشكال الرئيسية و سماحيتها للتشوه . هذا المقال يعرض منحنى جديد لإســتخلاص واصفات الشكل القائمة على المخطط الخارجى و الذى يتميز بالصغر و المرونة و الثبات أثناء عمليه تـصنيف الصور . كما أنه يمزج بين واصفات العزوم العامة و خصائص التحليل المتعدد للتحويل المويجى لإســتخلاص المعلومات التقريبية عن شكل الشيء . و بتكامل عملية التقسيم فى مخطط توليد الواصفات يصبح المنحنى المقدم قائم على الشيء . التجارب العملية أظهرت نتائج جيدة فيما يخص دقة تصنيف الصور الطبية .

Abstract

Foundation of a robust image classifier depends on having an accurate image's description based on its visual content. Recently, contour-based shape descriptors are employed for object-based representation due to its applicability to generic shapes and tolerance to noise and distortion. In this paper, an approach for extracting a hierarchical contour-based shape descriptor is described. It benefits compactness, flexibility, and suitability for image classification. This approach mingles the global description of moments with the multiresolution decomposition property of wavelet transform for robust shape representation and extracts approximate information about object's shape. Furthermore, by integrating a suitable segmentation algorithm into the descriptor generation schema, the proposed approach turns into object-based. Experimental results show that the resultant descriptor provides promising results in terms of accuracy for medical image classification.

1.Introduction

The irregular format of digital image tends to defy standard categorization and classification techniques. Classification problems generally, aim to identify the characteristics that indicate the group to which each instance belongs. Classification can be used both to understand the existing data and to predict how new instance will behave [1]. The benefits of image classification include better image storage and management, and optimized image-indexing scheme for fast and efficient image retrieval [2].

Traditional systems used to store and process multimedia images provide little to no means of automatic classification. Existing image retrieving systems [3, 4] limit classification mechanism to describing an image based on metadata such as color, texture, or shape features. Other systems use neural networks together with image features (descriptor) to provide automatic classification of images [5, 6]. Antonie et al [5] exploited the use of neural networks in classification of breast cancer image using back-propagation which proved to be less sensitive to database imbalance at a cost of high training time.

In medical application, shape is one of the most essential low-level images feature attributes that have received attention for classification [6]. Shape is a very significant feature in image perception. Human beings tend to perceive scenes as being composed of individual objects, which can be best identified by their shapes [7]. One main advantage of using the shape feature of a target is that it contains fewer parameters since it can be represented by one dimensional curve. Another advantage is that the shape feature can be normalized so that it has invariant properties. These properties greatly reduce the size of the target database and the complexity of target search algorithms [8]. In general, analysis of shapes requires the identification of proper descriptors that differentiate the shapes in the image for further classification and recognition.

Many researches on shape indexing and description have been proposed [9, 10, 11, 12]. These techniques can be classified into two distinct categories: contour based and region based shape description. The first one describes the considered region by using its external characteristics while the second one represents the considered region by using its internal characteristics. Adamrk et al [13] compared the various shape representation schemes. The comparison shows that contour-based shape properties are more significant for retrieval of semantically similar objects than region-based shape properties. The contour-based descriptor is very efficient in applications where high variability in the shape is expected, caused by, e.g., deformation in the object, and tolerant to noise presented in the contour [14].

Two major shape description methods are considered: Wavelet theory-based method and the Moment theory-based method. As far as the former approach is concerned, the wavelet transform is generally used to describe the shape from its boundary. Wavelet transform produces a sequence of coefficients called Wavelet descriptors (WD). These coefficients represent the shape of an object in the frequency domain where the lower frequencies symbolize its general contour, and the higher frequencies represent its detailed contour. Only a few coefficients are enough to describe even complex shapes. Wavelet descriptors have the advantage over Fourier descriptors in that, they achieve localization of shape features in joint-space. i.e., in both spatial and frequency domains. The wavelet transform's localization property concentrates on local differences between shapes within a limited set of coefficients [14].

The latter method uses region-based moments to characterize the contour of an object. It also considers global features such as center, variance, and symmetry. In general, this moment description is suited for a simple similarity search, but does not consider local contour variations, because it gives lower performance in the frequency domain. Thus, there have been efforts on incorporating another frequency-based technique to it for effective and compact contour representation. Babu et al [15] compared the performance of boundary-based representations, region-based representations and combined representations. Their experiments showed that combined representations outperformed any single representation.

Although system efficiency in terms of speed and computational complexity has been also subject of many researches, many related problems are still unsolved. A major shortcoming of the available shape description techniques is the lack of a sensible integration between segmentation and indexing when object-based description is envisaged. The research leading to this paper focuses on this problem, i.e. efficiency. The objective is to develop a scalable and efficient descriptor approach. This approach integrates a global moment's description and the wavelet hierarchical decomposition property, to form a contour-oriented representation tool of shapes. The approach is independent to object's translation, rotation, and scaling. This invariance is achieved by application of invariance transformation for the wavelet descriptor and the global nature of moment values for the moment descriptor. The generated descriptor is used in conjunction with neural networks to perform classification at various levels of detail.

This paper is organized as follows: Section 2 details the steps taken to extract contour descriptor. Section 3 introduces image modeling that depicts the proposed descriptor approach. Section 4 presents a system for medical image classification outlines the steps carried out by the neural network as it process an image. Selected results from the experimental evaluation are reported in section 5. Finally, the paper concludes with a summary in section 6.

2 Contour-based Feature Extraction

The following subsections outline the steps taken to successfully extract the contour features vector. Figure 1 shows the block diagram of extracting the wavelet-based contour descriptor.
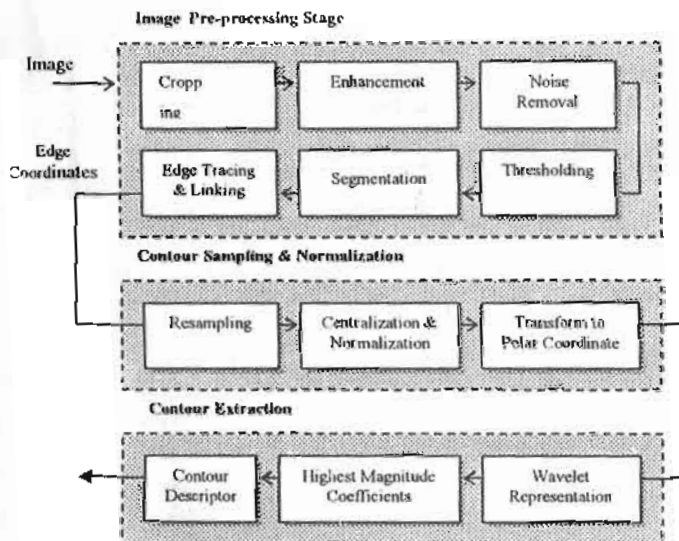

Fig.1 Steps of extracting the wavelet-based contour.

2.1 Pre-Processing Stage

Medical images are difficult to interpret, and a pre-processing stage is necessary to improve the quality of the images and make the feature extraction stage more reliable [5]. Three techniques are utilized in this work: a cropping operation, an image enhancement, and finally morphological noise removal. The first one is employed in order to remove the unwanted parts of the image usually peripheral to the area of interest. Image enhancement helps in qualitative improvement of the image with respect to a specific application.

In order to diminish the effect of over brightness or over darkness in the images and emphasize the image features, a widely used technique in the image processing to improve visual appearance known as histogram equalization is applied. Histogram equalization increases the contrast range in an image by increasing the dynamic range of the colors.

Regarding medical images, feature based on image object's shape can differentiate images better. Alas, the image quantization to black and white produces noise around the shape boundary, therefore, the use of de-noising process is vital. The de-noising process eliminates isolated pixels and isolated small regions or segments. In the developed approach, a morphological closing filter is used in order to remove noise, which can be defined as [10]:

$$B = B \bullet K = (B \oplus K) \otimes K .$$

where $\oplus$ and $\otimes$ are the morphological dilation operator and morphological erosion operator defined, respectively, by

$$B \oplus K = \bigcup_{k \in K}(k + B) \qquad B \otimes K = \bigcap_{k \in K}(k + B).$$

where K is the following 3 x 3 binary mask

$$K = \begin{bmatrix} 0 & 1 & 0 \\ 1 & 1 & 1 \\ 0 & 1 & 0 \end{bmatrix} \qquad (1)$$

an example of the three applied techniques is given in Figure2.
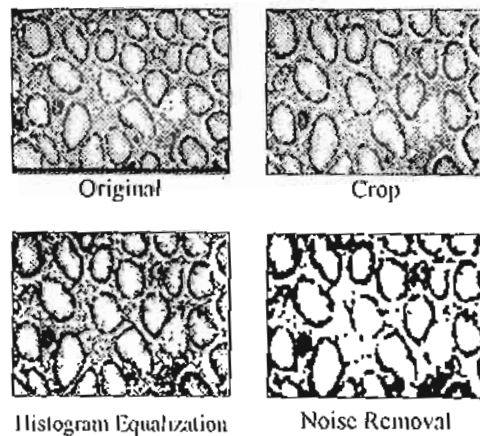

Fig2. Pre-processing stage on an example image.

2.2 Segmentation Stage

For the feature extraction of contour descriptor, segmented image material has to be provided. Medical images are rich in both color and texture, and a wide range of them can be considered as a mosaic of regions with different colors and textures [16]. In this work, segmentation is achieved by Expectation Maximization (EM) algorithm applied on a model based on Gaussian mixture distribution of the color and texture feature space [17]. After

running EM algorithm, each image pixel is labeled with the cluster values for which it attains the highest likelihood. A 3×3 max-vote filter is then applied to smooth the image and run a connected component algorithm to produce a set of homogeneous image regions (classes). Figure.3 gives an example of EM segmentation result with two classes.

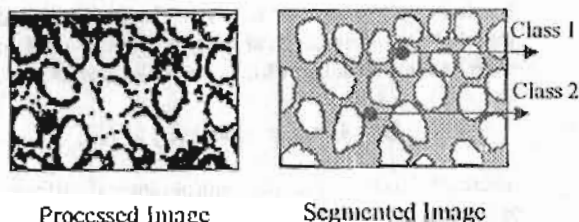Processed Image   Segmented Image

Fig.3. Example of segmented image.

2.3 Contour Representation and Sampling

Edge detection and edge tracing are very important tasks in contour features extraction. Technically, edge detection is the process of locating edge pixels, and edge tracing is the process of following the edges [17]. In a first step an ordered sequence of contour points approximating the input shape is extracted. For this purpose, a contour detection algorithm similar to that of Canny [18] is applied to the segmented image. For some shapes, the shape boundary is not always connected; therefore a clockwise edge-linking algorithm is used to fill the gaps between boundary points and to ensure that a closed contour is extracted from the image [19].

In the next step, a vector of equally distributed points along the curve is extracted from the ordered sequence of contour pixels (sampling process). The sampling process not only normalizes the sizes of shapes but also has the effect of smoothing the shape [19]. The smoothing eliminates the noise in the shape boundary and the small details along the shape boundary as well. By varying the number of sampled points, the accuracy of the shape representation can be adjusted. The technique used begin with sampling the edge coordinates using a uniform number of points so that no matter how long a curve is, the number of sampling points is the same, this property is crucial for scale invariance. If there are m original edge points $(x_o(i), y_o(i))$, $i = 0, 1,..., m-1$. The incremental curve length can be calculated as [20]:

$$l(0) = 0,$$

$$L = [x_o(i) - x_o(i-1)]^2 + [y_o(i) - y_o(i-1)]^2,$$

$$l(i) = l(i-1) + \sqrt{L}, \qquad i = 1,...,m \qquad (2)$$

The total length of the curve is denoted by $L = l(m)$. The curve is then uniformly sampled at n points, i.e.

$$x_n(j) = x_o(s)(1 - f) + x_o(s + 1)f,$$

$$y_n(j) = y_o(s)(1 - f) + y_o(s + 1)f, \qquad j = 1,...,m$$

with

$$s = \lfloor L \times J / n \rfloor, \qquad f = \frac{L \times j/n - l(s)}{l(s+1) - l(s)} \qquad (3)$$

From this point, the contour of the shape is presented by the ordered sequence $(x(s), y(s))$ of contour points, where s denotes the position along the contour. In order to facilitate the use of the fast wavelet transform. The number of sampled points is chosen to be power of two

2.4 Contour Normalization

Shape must be normalized before wavelet transform is performed. Edge coordinates are in general dependent on the displacement, scaling, and rotation of the target. A normalization process is performed so that the normalized edge coordinates have 2D shift, scale, and rotation invariant properties. To normalize the contour representation with respect to displacement, the curve is shifted so that the center of the curve is located at the origin. This is achieved by calculating the new coordinates $(x_n(j), y_n(j))$, using

$$x_n(j) = x(j) - \bar{x}, \qquad y_n(j) = y(j) - \bar{y} \qquad (4)$$

where $(\bar{x}, \bar{y})$ is the mean of the edge coordinates. To normalize the representation with respect to scaling and 2D rotation, edge points are transformed from Cartesian coordinates to Polar coordinates via

$$R(j) = \sqrt{x_n(j)^2 + y_n(j)^2},$$

$$\theta(j) = \tan^{-1}\left(\frac{y_n(j)}{x_n(j)}\right) \qquad (5)$$

R(j) is then normalized so that it has the unit radius. Since all targets with different sizes have the same radius, they are scale-invariant. Finally, for rotational invariance, the coordinates are rotated so that the center of mass $\sum i \tilde{R}_k(i)$ for radius R is minimized [19].

$$\tilde{R}_k(i) = \begin{cases} R(i + k) & 0 \le i < N - k \\ R(i - N + k), & N - k \le i < N \end{cases}$$

where

$$k = \arg\min_{k} \sum_{i=1}^{N} i\widetilde{R}_k(i). \qquad (6)$$

2.5 The Wavelet Descriptor

The wavelet transform is a tool that divides up data, functions, or operators into different frequency components and then studies each component with a resolution matched to its scale [20]. Therefore, the wavelet transform is anticipated to provide informative mathematical representation of many objects of interest. Wavelets have many favorable properties, such as vanishing moments, hierarchical and multiresolution decomposition structure, dilating relation, compactness of the support, decelerated coefficients, and a wide variety of basis functions [1, 21]. These properties provide considerably more efficient and effective solutions to many shape description problems.

Let $\{Z_i^2\}$ be a discrete parameterised closed planar curve-that represents the contour of an object of interest consisting of N points (obtained in previous section) of the form [20] [1]

$$\{Z_i^2\} = \begin{bmatrix} \{R_i\} \\ \{\Phi_i\} \end{bmatrix} \quad ,$$

or also, in matrix notation

$$Z^2 = \begin{bmatrix} R \\ \Phi \end{bmatrix} \qquad (7)$$

where the parameter i corresponds to the normalized arc length. If a level J_o partial one-dimensional "Discrete Wavelet Transform" (DWT) is applied independently to each component, the planar curve can be described in terms of the multiresolution analysis of $\{R_i\}$ and $\{\Phi_i\}$:

$$Z^2 = \begin{bmatrix} R \\ \Phi \end{bmatrix} = \begin{bmatrix} w^T W_R \\ w^T W_{\Phi} \end{bmatrix}$$

$$= \begin{bmatrix} v_{J_o}^T V_{RJ_o} \\ v_{J_o}^T V_{\Phi J_o} \end{bmatrix} + \sum_{j=1}^{j_o} \begin{bmatrix} w_j^T W_{Rj} \\ w_j^T W_{\Phi j} \end{bmatrix} \qquad (8)$$

where w is an $N \times N$ real-valued matrix defining the partial DWT, and W_R, W_{Φ} are column vectors of length N in which the first $(1 - 2^{-J_o})N$ elements are the wavelet coefficients, and the last $2^{-J_o}N$ elements are the scaling coefficients. The $w_j^T W_{Rj}$, $j = 1, 2, \ldots, J_o$ are the detail vector whose elements are

related to changes in the R component at scale 2^{J-1}, and the smooth vector $v_{j_o}^T V_{RJ_o}$ represents averages at scale 2^{J_o}. The *wavelet descriptor* (WD) for the planar curve Z^2 is defined as the coefficients of the partial DWT for R and Φ, that is

$$WD(Z^2) = \begin{bmatrix} W_R \\ W_{\Phi} \end{bmatrix} \qquad (9)$$

With this definition, a multiresolution representation of the closed curve has been obtained by using only a subset of wavelet coefficients consisting of primarily coarser scale components. In general, the two properties of wavelets that are exploited for shape characterization are the capability for detecting and representing local features, and the energy compaction in the transformed coefficients that make the description process more effect and accurate [1].

According to [22], the R-component of the contour points is most important, while the influence of Φ-component could be neglected. Therefore, a contour is represented by a single one-dimensional wavelet transform W_R. Because, the most important wavelet coefficients are the ones describing the lowest frequencies, only the first 10 coefficients are used as wavelet-based contour descriptor.

2.6 Global Descriptor of Moment

The distribution of different regions is a global feature used to characterize the image content. Thus, one way to apply this global feature is storing information for each region separately, such as its positions and sizes. In this work, the features to be considered as global descriptor are: Dispersion (see Eq.10) and Modification ratio (see Eq.11)[23]. Assume that the result of segmenting image I is the image S, and that the pair (x, y) represents a spatial location. The mass of the contour labeled with the class c after the segmentation is given by:

$$m_c = \sum_s h_c(x, y) \qquad .$$

where

$$h_c = \begin{cases} 1 & if \quad S_{x,y} \in c \\ 0 & if \quad S_{x,y} \notin c \end{cases} \quad .$$

the center of mass (centroid) of the contour labeled as c is given by:

---

[1] In this paper, $\{Z_i^2\}$ indicates that Z is bi-dimensional, not power operations. The same holds for matrix notation.

$$x_c = \frac{\sum_{x,y} x.h_c(x,y)}{m_c} \quad, \quad y_c = \frac{\sum_{x,y} y.h_c(x,y)}{m_c},$$

The *dispersion* feature is a summation of distances. Therefore, for each contour i, the centroid is computed and then their distances to the global class canter (x_c, y_c) are summed as follows:

$$d_c = \sum_i \sqrt{(x_c - x_i)^2 + (y_c - y_i)^2} \qquad (10)$$

The *modification ratio* is defined by the ratio of inscribed diagonal d_i that has the same second-moments as the region, to maximum diagonal d_m. This value describes whether a contour is thin (oval like) or circular. The parameters inscribed and maximum diagonal, represent the dimensions of surrounding rectangle, as depicted in Figure 4.

$$Modification\ ratio = \frac{d_i}{d_m} \qquad (11)$$

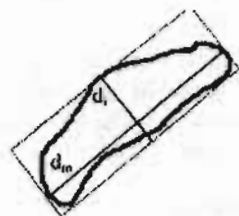
Fig. 4: Contour with associated diagonals

3 Image Mathematical Modeling

An image is mathematically modeled according to a so-called object model O to describe the content of image regions [24]. Every image region is specified by an image object O_n of type O, with $n=1,...., N$. The image is modeled as:

$$M=(d, O_n),$$

where d is the dispersion, and O is defined by the following 2-tuple:

$$O =(W, G) \qquad (12)$$

where W presents the wavelet feature values, and G *presents* the moment feature values. Following the definition of image descriptors, which consist of the wavelet-based feature vector and the modification ratio per image region, plus the dispersion for entire image, each vector is associated with an index that corresponds to a particular category.

4 Descriptor Accuracy Evaluation

A system is developed for testing purposes. In this system, the contour-based shape descriptor extractor is followed by a "Learning Vector Quantization" neural network classifier for object identification based on its content. This system circumvents the low precision classification technique of other systems [5, 6] by examining the actual objects within an image and using them to discover relationships that reveal information useful in classifying the entire image, Figure 5 shows an overview of the classification system.
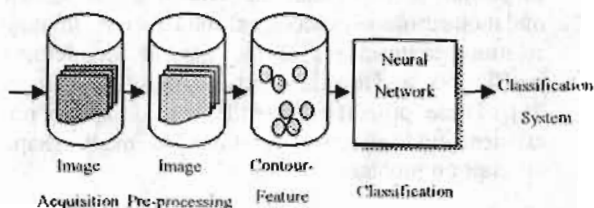

Fig.5. Architecture of the Evaluation system.

Kohonen learning vector quantization [25] (LVQ) is a supervised algorithm for training. Vector Quantization classifier rapidly converges to a "good" solution. It generates a table of vector templates known as a *codebook*. Each codebook vector is associated with a category. During classification, the Euclidean distance between the input vector and all of the codebook vectors are computed. The input vector is assigned to the class corresponding to the nearest codebook vector. A neural network architecture implementing these operations is shown in Figure 6, where R = number of elements in input vector , S^1 = number of competitive neurons and S^2 = number of linear neurons. For more details, see [25].
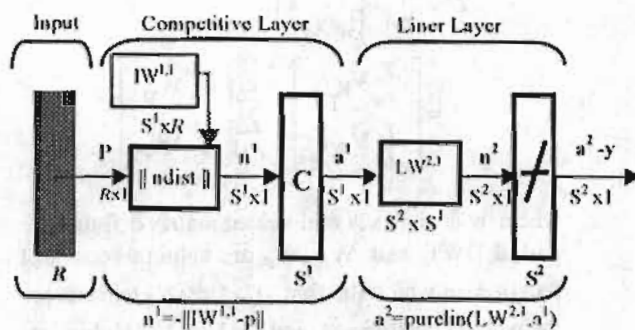

Fig.6. Neural network architecture for the LVQ algorithm [25].

For the evaluation, samples of morphological medical images are selected from the faculty of

medicine, university of Alexandria. This images show microscopic appearance of normal mucosa of the colon (Transverse section, H&E x400). Sixty five percent of which are used to train the neural network, while the rest are used to test the trained network. Five different network configurations are developed. The configuration parameters are: RMS is the root mean square error that employs to adjust the weights between network layers in order to correctly classify the training images, NC is the number of feature vector coefficients for each region as explained in section 3, and CR is the classification rate. After training of each neural network configuration, it is tested on all the images using the contour-shape descriptor. Table 1 shows the result of the testing the five configurations.

Table1. Results from five neural network configurations of the LVQ Classifier.

Network Configuration	RMS	NC	CR (%)
1	0.045	31	83.75
2	0.023	11	85.83
3	0.023	16	87.8
4	0.034	21	85.83
5	0.031	25	87.69

The second configuration delivers the highest classification rate, although it uses a lower numbers of feature vectors. Since the classification process is performed using non-complex contour descriptor, the classification time remains almost constant when the database grows.

To justify the results obtained from this study, the LVQ classifier has been compared with three other classifiers: K-means classifier, Multiple Layers Perceptron (MLP), and the Support Vector Machine (SVM). Using the same training image sets, and the same contour vector is fed to the classifiers. The results of testing the classifier can be founded in Figure 7.
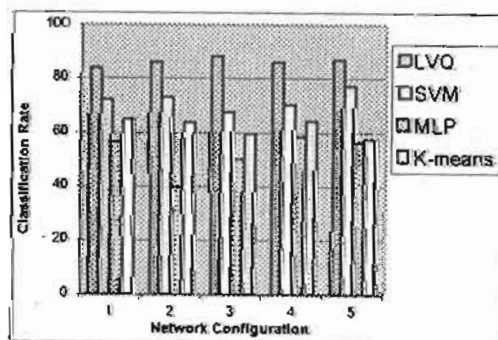
Fig.7. Results from the other three classifiers plus LVQ classifier.

The results obtained indicate that the LVQ compared favorably with three other classifiers and outperformed them on average by 15 %.

5 Conclusions

In this paper, an integrated contour-based shape description approach that demonstrates the feasibility of using wavelet transform with global description of moments for automatic medical images classification is presented. It is shown that descriptor defined from contour features extracted during the segmentation is very suitable for object-based description. Image objects are represented with a small number of the largest magnitude wavelet coefficients that describe the local features for each contour and global features of moments allowing for an efficient contour representation.

The developed descriptor is compact and flexible abstraction that inherently fits any classification strategy. The techniques of target contour extraction from the pathological medical images and the shape normalization for 2-D shift, scale, and rotation invariance are also described.

The advantages of using the developed shape descriptor are threefold. First, the descriptor represents well each region's overall color and texture distribution because they are based on the features generated by the segmentation algorithm. Second, the shape descriptor is compact: the contour-features distribution of each region is summarized by approximately 11 values. Finally, the descriptor is flexible abstractions for which it can define a hierarchical classification strategy. This strategy is performed by varying the number of wavelet coefficients used to describe the contour. Experimental evaluation of the developed descriptor shows its effectiveness.

References

[1] Tao Li, Qi Li, S. Zhu, and M. Ogihara, "A Survey on Wavelet Applications in Data Mining ". In Proc. of SIGKK Explorations, Vol.4, Issue 2, pp.49-63, 2002.

[2] J. Zhang, W. Hsu, and M. L. Lee, "Image Mining: Trends and Development", Technical Report, School of Computing, National University of Singapore, 2002

[3] F. M. Sawhney, H. Niblack, and J. Lee, "The QBIC Project: Querying Images By Content Using Color, Texture and Shape", SPIE Conf. on Storage and Retrieval for Image and Video Databases, Vol. 1908, pp.173-187, 1993.

[4] Peter Stanchev, "Content-Based Image Retrieval Systems", CompSysTech'2001, 21-22.06.2001, Sofia, Bulgaria, 2001.

[5] M. L. Antonie, O.R. Zainne, and A. Coman, "Application of Data Mining Techniques for Medical Image Classification", Proceedings of the Second International Workshop on Multimedia Data Mining, USA, August 2001.

[6] C. Breen, L. Khan, A. Kumar, and L. Wang, "Ontology- Based image Classification using Neural Networks", In Proc. of SPIE, 2002.

[7] D. Tegolo, "Shape Analysis for Image Retrieval", Proc. of Storage and Retrieval for Image and Video Databases-II, No. 2185, San Jose, pp. 59-69, February 1994.

[8] J.E. Gary and R. Mehrotra, "Shape Similarity-based Retrieval in Image Database", Proc. of SPIE, Image Storage and Retrieval Systems, Vol.1662, pp. 2-8, 1992.

[9] F. Ghorbel, "A Complete and Stable Set of Invariant Fourier Descriptors for Random Planar Shape", International Conference on Image Processing and its Applications, pp.278-281, 1992.

[10] S. Kon'ya and K. Kushima, "A Rotation Invariant Shape Representation based on Wavelet Transform", Challenge of Image Retrieval, Newcastle Upon Tyne, 1998.

[11] F. Mokhtarian, S. Abbasi, and L. Kittler, "Efficient and Robust Retrieval by Shape Content Through Curvature Scale Space", Image Databases and Multimedia Search, pp.51-58, 1997.

[12] S. Belongie and J. Puzicha, "Shape Context: A New Descriptor for Shape Matching and Object Recognition", Technical Report, University of California at Berkeley, USA, 2000.

[13] T. Adamrk and N. O'connor, "Efficient Contour-based Shape Representation and Matching", MIR'03, Nov. 7, Berkeley, California, USA, 2003.

[14] D. Zhang and Guojun Lu, "A Comparative Study on Shape Retrieval Using Fourier Descriptors With Different Shape Signatures", Technical Report, Monash University, Australia, 1999.

[15] Babu M. Mehtre and Wing F. Lee, "Shape Measures for Content based Image Retrieval: A Comparison", Information Processing & Management, 33(3), 1997.

[16] K.S. Magoulas, and G. D. Grigoriadou, "Detecting Abnormalities in Colonoscopic Images by Textural Description and Neural Network", In Proc. of Work on Mach. Learn. In Med. Appl., Greece, 1999:59-62.

[17] T. Y. Lui and E. Izquierdo, " Scalable Object-based Image Retrieval", In Proc. of International Conf. of Image Processing (ICIP), 2003.

[18] Canny J., "A computational approach to edge detection", IEEE Transactions on Pattern Analysis and Machine Intelligence, PAMI-8 (6), 679-698, 1986.

[19] Jin Li and C.C. Jay Kuo, "Automatic Target Shape Recognition via Deformable Wavelet Template", Technical Report, Signal and Image Processing Institute, University of Southern California, Los Angeles.1995.

[20] D. G. Perez and F. G. Ugalde, "Compact Representation of Planar Curves based on Wavelet Shape Descriptor for Multimedia Applications", Vision Interface'99, Trois-Rivieres, Canada, 19-21 May.

[21] F. A. Cheikh, A. Quddus, and M. Gabbouj, "Shape Recognition based On Wavelet Transform Modulus Maxima", IEEE Transactions on Image Processing, 2000.

[22] J. Ohm, B. Makai, and A. Smolic, "A Set of Visual Feature Descriptors and their Combination in a Low-Level Description Scheme", Technical Report, Heinrich Hertz Institute, Image Processing Department, Germany, 1999.

[23] A. J. M. Traina, A. R. Balan, and C. T. Jr, "Content-based Image Retrieval Using Approximate Shape of Objects", Proc. IEEE Int. Conf. on Multimedia and Expo, 2004.

[24] T. Kampfe, T. Kaster, and H. Ritter, "Adaptive Content-based Image Retrieval by Combining Feature Weighting and Query Refinement", Applied to Computer Science Group, Faculty of Technology, University of Bielefeld, Germany, 2001.

[25] M. Blume, and D. R. Ballard, "Image Annotation based on Learning Vector Quantization and Localized Haar Wavelet Transform Features", Technical Report, Reticular Systems Inc. San Diego, CA, 1998.